Article

Journal of Vibration and Control
1–15

DOI: 10.1177/1077546315575434
jvc.sagepub.com

Local impact analysis for deck slabs of prestressed concrete box-girder bridges subject to vehicle loading

Yang Yu[1,2], Lu Deng[1,3], Wei Wang[1] and CS Cai[2]

Abstract

In bridge design codes, the dynamic impact factor (IM) is a well-accepted measure of the impact effect of vehicular loads on bridges. Many previous studies focused on the evaluation of IMs based on the global responses of the main girders while little attention was paid to the local impact effect on bridge decks. As a result, the IMs specified in many design codes, which were traditionally derived from the global responses of bridges, may not be necessarily reasonable for the design of deck slabs. This study was intended to investigate the local impact effect of vehicular loads on the deck slabs of prestressed concrete box-girder bridges. A bridge-vehicle coupled model was adopted to calculate both the local and global IMs. The obtained local and global IMs were compared and the relationship between the IM and three important parameters, including the road surface condition, vehicle speed, and bridge span length, was studied. The results showed that there was no strong correlation between the global and local IMs; however, the local IMs were well correlated with the road surface condition and bridge span length. A discussion on the impact provisions in different bridge codes was also presented.

Keywords

Local impact factor, vehicle-bridge interaction, bridge deck, road surface condition, vehicle speed, bridge span length

1. Introduction

Vehicle-induced vibration is one of the primary concerns in bridge engineering. It is well accepted that a moving vehicle will exert a dynamic impact on bridges, usually causing an increase in the bridge's responses over the corresponding static ones. In bridge design codes, the dynamic impact effect is usually accounted for by using a dynamic impact factor (IM). Accurate evaluation of the IM plays a critical role in the design and evaluation of bridges since a reasonable IM leads to safer and more economical designs of new bridges and provides valuable information for the condition assessment and management of bridges in service. It is noted that other similar terminologies, such as the dynamic amplification factor (DAF) and dynamic load factor (DLF), have been used in the literature and will be cited below.

Numerous studies have been conducted to investigate the dynamic effect of moving vehicles on bridges, including both field tests and numerical simulations. However, most previous studies focused on the global responses of the main structural components such as the main girders (Huang et al., 1993; Huang et al., 1995; Wang et al., 1996); few studies have been carried out to examine the impact effect of vehicular loads on the local structural components. Broquet et al. (2004) investigated the dynamic behavior of the deck slabs of concrete highway bridges and calculated the DAF for different responses of deck slabs under vehicle loading. The results suggested that DAFs do not vary significantly between different locations on a deck slab. However, no comparison was made between the DAFs of local deck responses and global bridge responses.

Furthermore, the applicability of the global impact provisions in some bridge design codes to the local design of bridge decks has not been justified. The IMs

[1]College of Civil Engineering, Hunan University, Changsha, Hunan, China
[2]Department of Civil and Environmental Engineering, Louisiana State University, Baton Rouge, Louisiana, USA
[3]Key Laboratory for Wind and Bridge Engineering of Hunan Province, Hunan University, Changsha China

Received: 10 October 2014; accepted: 5 February 2015

Corresponding author:
Lu Deng, College of Civil Engineering, Hunan University, Changsha, Hunan, China.
Email: denglu@hnu.edu.cn

in some design codes were traditionally derived from the measurement or simulation of global bridge responses. For example, the impact provision in the AASHTO LRFD code (AASHTO, 1994) is based on the work by Hwang and Nowak (1991) in which the deflection at the bridge mid-span was used to calculate the DLF. However, the controlling internal force of the bridge deck is the transverse bending moment of which the dynamic increment may not be accurately represented by the IM of global bridge responses. As a result, it may be unreasonable to apply the IMs in some bridge design codes to the local design of bridge decks. It is therefore necessary to conduct an in-depth investigation regarding the local impact effect of moving vehicles on bridge deck slabs.

This study presents a local impact analysis for the deck slabs of prestressed concrete box-girder bridges under vehicular loads based on numerical simulations. A three-dimensional (3D) vehicle-bridge coupled model was adopted to compare both the global bridge responses and local responses of the deck slabs in terms of the dynamic impact factor. A parametric study was then conducted to investigate the relationship between the IM and three important parameters including the bridge span length, road surface condition, and vehicle speed. Finally, the impact provisions in different bridge codes were discussed based on the obtained results.

2. Numerical models

2.1. Prototype of the bridge

In the present study, five typical box-girder bridges with span lengths ranging from 24 m to 58 m were selected according to the Segmental Box Girder Standards by the AASHTO-PCI-ASBI (1997). These bridges are good representatives of the simply-supported prestressed concrete box-girder bridges in the United States. All five bridges have the same cross-section and have two end diaphragms with a thickness of 0.40 m. The girder depth and deck width of the bridges are 2.4 m and 11.1 m, respectively. A typical cross section of bridges is shown in Figure 1. It should be noted that while larger thickness of bottom slabs is usually adopted near the piers, it has little effect on the natural frequencies of the bridge. Thus, the bridges were modeled with constant cross-sections throughout the span in this study. The selected bridges were modeled with the ANSYS software using solid elements (with three translational degrees-of-freedom at each node) to predict the fundamental dynamic characteristics, such as natural frequencies and mode shapes. Figure 2 shows the finite element model of Bridge 2. It should be noted that the barrier of the bridge were simplified by increasing the density of the materials on the two sides of the bridge deck. The geometric properties and fundamental frequencies of the five bridges are shown in Table 1.

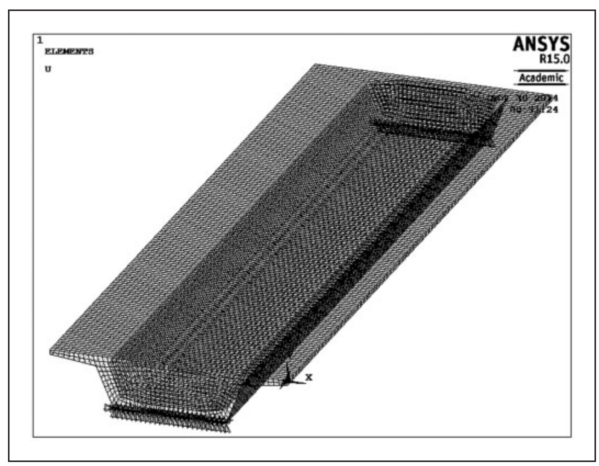

Figure 2. Finite element model for Bridge 2 in ANSYS.

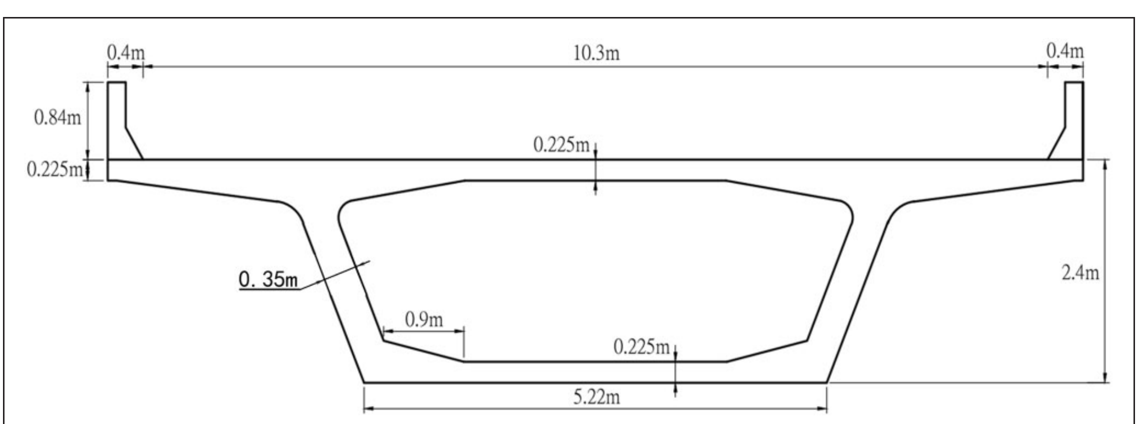

Figure 1. Typical cross-section of bridges.

2.2. Prototype of the vehicle

In this study, a major design vehicle in the AASHTO bridge design specifications, i.e., the HS20-44 truck, was adopted for the vehicle loading. The analytical model of the truck is shown in Figure 3. The vehicle bodies (tractor and trailer) were represented by rigid bodies with mass and three DOFs, i.e., vertical displacement, pitching rotation, and rolling rotation. Each wheel was represented by a lumped mass with one DOF, i.e., vertical displacement. All together, the vehicle model consists of eleven independent DOFs. The detailed geometric and mechanical properties of the truck are shown in Table 2 (Wang and Liu, 2000; Deng and Cai, 2010). The modal frequencies of the vehicle were calculated as 1.52, 2.14, 2.69, 5.94, 7.74, 7.82, 8.92, 13.87, 13.99, 14.63, and 17.95 Hz, respectively.

2.3. Road profile model

In the AASHTO LRFD code (AASHTO, 2012), road surface irregularity is regarded as a main cause of the dynamic effect of moving vehicles. Generally speaking, in numerical simulations a road profile is usually represented by a zero-mean stationary random process that can be expressed by a power spectral density (PSD) function. In this study, a modified PSD function (Wang and Huang, 1992) was used

$$\varphi(n) = \varphi(n_0)\left(\frac{n}{n_0}\right)^{-2} \quad (n_1 < n < n_2) \tag{1}$$

where n is the spatial frequency (cycle/m); n_0 is the discontinuity frequency of 0.5π (cycle/m); $\varphi(n_0)$ is the roughness coefficient (m^3/cycle); and n_1 and n_2 are the lower and upper cut-off frequencies, respectively. The International Organization for Standardization (ISO, 1995) classified the road surface condition into a few categories based on different values of roughness coefficient. In the present study, according to ISO specifications (ISO, 1995), the roughness coefficients of 5×10^{-6}, 20×10^{-6}, 80×10^{-6}, and $256 \times 10^{-6}\,\mathrm{m}^3$/cycle were used for very good, good, average, and poor road surface conditions, respectively.

The road surface elevation can then be generated by an inverse Fourier transformation as

$$r(x) = \sum_{k=1}^{N} \sqrt{2\varphi(n_k)\Delta n}\cos(2\pi n_k x + \theta_k) \tag{2}$$

where θ_k is the random phase angle uniformly distributed between 0 and 2π; n_k is the wave number (cycle/m); N is the number of frequencies between n_1 and n_2; and Δn is the frequency interval between n_1 and n_2.

Table 1. Primary data of the five bridges.

Bridge number	Span length (m)	Fundamental frequency (Hz)	Cross-section at mid-span: Area (m^2)	Cross-section at mid-span: Moment of inertia (m^4)
1	24	7.92	6.395	5.085
2	32	4.70		
3	40	3.09		
4	48	2.18		
5	56	1.61		

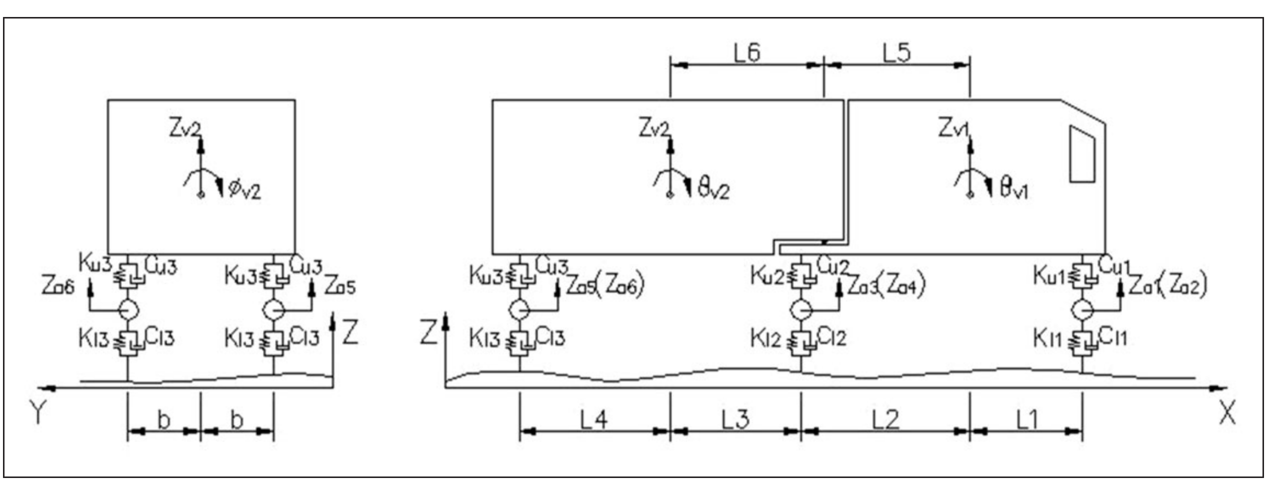

Figure 3. Analytical model of the HS20-44 truck.

Table 2. Major parameters of the HS20-44 truck.

Items	Parameters	Values
Geometry	L1	1.698 (m)
	L2	2.569 (m)
	L3	1.984 (m)
	L4	2.283 (m)
	L5	2.215 (m)
	L6	2.338 (m)
	b	1.1 (m)
Mass	Truck body 1	2612 (kg)
	Truck body 2	26113 (kg)
	First axle suspension	490 (kg)
	Second axle suspension	808 (kg)
	Third axle suspension	653 (kg)
Moment of inertia	Pitching, truck body1	2022 (kg m^2)
	Rolling, tuck body 1	8544 (kg m$^{2)}$
	Pitching, truck body 2	33153 (kg m^2)
	Rolling, tuck body 2	181216(kg m^2)
Spring stiffness	Upper, first axle	242604 (N/m)
	Lower, first axle	875082 (N/m)
	Upper, second axle	1903172 (N/m)
	Lower, second axle	3503307 (N/m)
	Upper, third axle	1969034 (N/m)
	Lower, third axle	3507429 (N/m)
Damper coefficient	Upper, first axle	2190 (N s/m)
	Lower, first axle	2000 (N s/m)
	Upper, second axle	7882 (N s/m)
	Lower, second axle	2000 (N s/m)
	Upper, third axle	7182 (N s/m)
	Lower, third axle	2000 (N s/m)

3. Vehicle-bridge interaction system

The interaction between the vehicle and bridge can be solved by using either an iterative procedure (Broquet et al., 2004) or a coupled method (Deng and Cai, 2010). In the present study, a coupled method was used. The two sets of equations of motion for the vehicle and bridge can be written in matrix forms as

$$[M_v]\left\{\ddot{d}_v\right\} + [C_v]\left\{\dot{d}_v\right\} + [K_v]\{d_v\} = \{F_G\} + \{F_v\} \tag{3}$$

$$[M_b]\left\{\ddot{d}_b\right\} + [C_b]\left\{\dot{d}_b\right\} + [K_b]\{d_b\} = \{F_b\} \tag{4}$$

where $[M_v]$, $[C_v]$, and $[K_v]$ = the mass, damping, and stiffness matrices of the vehicle, respectively; $[M_b]$, $[C_b]$, and $[K_b]$ = the mass, damping, and stiffness matrices of the bridge, respectively; $\{d_v\}$ and $\{d_b\}$ = the displacement vector of the vehicle and bridge, respectively; $\{F_G\}$ = the gravity force vector of the vehicle; and $\{F_v\}$ and $\{F_b\}$ = the wheel-road contact force vectors acting on the vehicle and bridge, respectively.

Based on the displacement relationship and interaction force relationship at the contact points, the two sets of equations of motion above can be combined into one coupled equation

$$\begin{bmatrix} M_b & \\ & M_v \end{bmatrix}\begin{Bmatrix} \ddot{d}_b \\ \ddot{d}_v \end{Bmatrix} + \begin{bmatrix} C_b + C_{b-b} & C_{b-v} \\ C_{v-b} & C_v \end{bmatrix}\begin{Bmatrix} \dot{d}_b \\ \dot{d}_v \end{Bmatrix} + \begin{bmatrix} K_b + K_{b-b} & K_{b-v} \\ K_{v-b} & K_v \end{bmatrix}\begin{Bmatrix} d_b \\ d_v \end{Bmatrix} = \begin{Bmatrix} F_{b-r} \\ F_{b-r} + F_G \end{Bmatrix} \tag{5}$$

where C_{b-b}, C_{b-v}, C_{v-b}, K_{b-b}, K_{b-v}, K_{v-b}, F_{b-r}, and F_{b-r} are the interaction terms caused by the contact forces. As the vehicle moves across the bridge, the positions of contact points change and so do the contact forces. Thus, the interaction terms are time-dependent terms and will change as the vehicle moves across the bridge.

In order to reduce the size of the matrices and therefore save calculation efforts, the modal superposition technique was employed; the bridge displacement vector $\{d_b\}$ in equation (5) can be expressed as

$$\{d_b\} = \left[\{\Phi_1\} \quad \{\Phi_2\} \ldots \{\Phi_m\}\right]\left\{\xi_1 \quad \xi_2 \cdots \xi_m\right\}^T = [\Phi_b]\{\xi_b\} \tag{6}$$

where m = the total number of modes considered for the bridge; $\{\Phi_i\}$ and ξ_i = the ith mode shape of the bridge and the ith generalized modal coordinate, respectively. If each mode shape is normalized such that $\{\Phi_i\}^T[M_b]\{\Phi_i\} = 1$ and $\{\Phi_i\}^T[K_b]\{\Phi_i\} = \omega_i^2$ and the damping matrix $[C_b]$ in equation (4) is assumed to be equal to $2\omega_i\eta_i[M_b]$, where ω_i and η_i = the natural circular frequency and the percentage of the critical damping of the ith mode of the bridge, respectively, then equation (5) can be simplified as

$$\begin{bmatrix} I & \\ & M_v \end{bmatrix}\begin{Bmatrix} \ddot{\xi}_b \\ \ddot{d}_v \end{Bmatrix} + \begin{bmatrix} 2\omega_i\eta_i I + \Phi_b^T C_{b-b}\Phi_b & \Phi_b^T C_{b-v} \\ C_{v-b}\Phi_b & C_v \end{bmatrix}\begin{Bmatrix} \dot{\xi}_b \\ \dot{d}_v \end{Bmatrix} + \begin{bmatrix} \omega_i^2 I + \Phi_b^T K_{b-b}\Phi_b & \Phi_b^T K_{b-v} \\ K_{v-b}\Phi_b & K_v \end{bmatrix} \times \begin{Bmatrix} \xi_b \\ d_v \end{Bmatrix} = \begin{Bmatrix} \Phi_b^T F_{b-r} \\ F_{v-r} + F_G \end{Bmatrix} \tag{7}$$

The coupled equation (7) contains only the modal properties of the bridge and the mechanical parameters

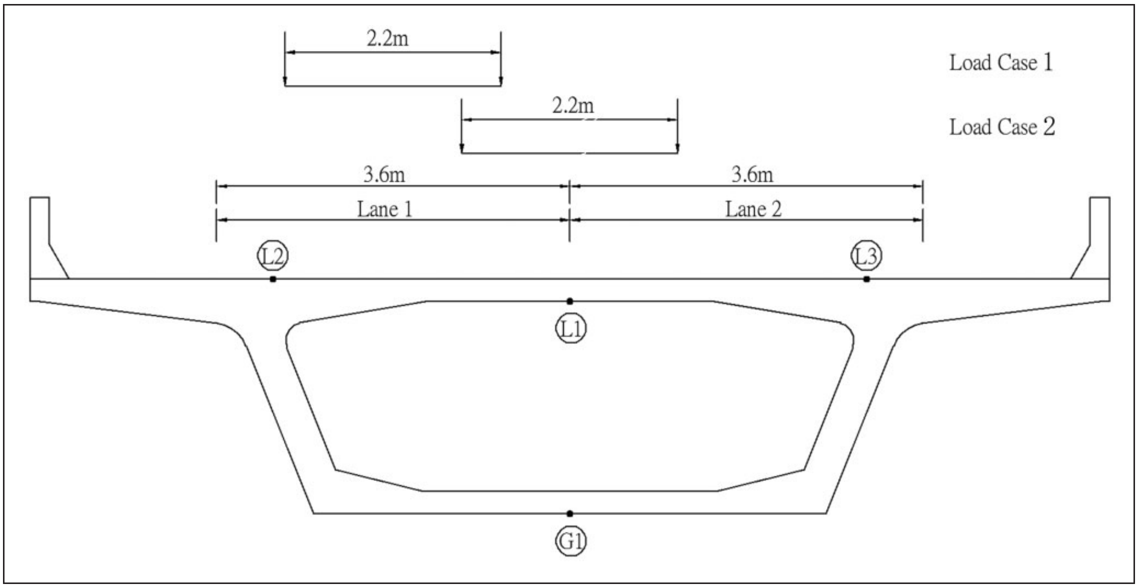

Figure 4. Selected locations for the calculation of IM and vehicle loading positions.

of the vehicles. As a result, the complexity of solving the coupled equations was greatly reduced. A computer program was developed in the MATLAB environment to solve equation (7) in the time domain using the fourth-order Runge-Kutta method. After obtaining the displacement responses of the bridge $\{d_b\}$, the strain responses can be obtained by

$$\{\varepsilon\} = [B]\{d_b\} \tag{8}$$

where $[B]$ = the strain-displacement relationship matrix assembled with the x, y, and z derivatives of the element shape functions.

4. Numerical analysis

4.1. Selection of bridge responses and definition of dynamic impact factor

In the present study, the responses at seven locations of each bridge were evaluated. Figure 4 shows the selected locations at the bridge mid-span whose responses were used for the calculation of IMs. Among these locations, L1, L2 and L3 were the control locations for the transverse bending moment and thus the transverse strain at these locations were calculated; G1 was the control location for the longitudinal bending moment and thus the longitudinal strain as well as the vertical displacement at these locations were predicted. Similarly, three locations at the quarter-span (L4, L5 and L6) that correspond to the locations of L1, L2 and L3 at the mid-span cross-section were selected as well. These seven locations were considered such that L1 to L6 represent the local responses of the deck slab while G1 represents the global response of the bridge. As a result, the responses of seven points (eight responses) were evaluated for each bridge. It should be mentioned that the reason for not considering the global response at the quarter span was that the global response at the mid-span was larger than that at the quarter-span. Similarly, the transverse strain responses at the support were not considered either due to the reason that the transverse strains at the support were smaller than those at the mid-span and quarter-span. Furthermore, two load cases were considered in this study. Figure 4 shows the transverse positions of the vehicle for the two load cases in which a single truck was set to travel along the centerline of Lane 1 and the centerline of the deck slab, respectively. Load Case 1 represents a common loading scenario for highway bridges while Load Case 2 produces the maximum local responses at the control locations of the deck slab (such as L1, L2, and L3).

As discussed earlier, the dynamic impact factor (IM), also known as the dynamic load allowance (DLA), is usually adopted in bridge designs to account for the dynamic load increment from the static load effect. In the present study, the IM was defined as

$$IM = \frac{R_{dyn} - R_{sta}}{R_{sta}} \tag{9}$$

where R_{dyn} and R_{sta} are the maximum dynamic and static responses of the bridge at a given location, respectively.

In the development of some bridge design codes, the IM was traditionally derived from the global dynamic responses. In this paper, the IM at the location G1 was defined based on the global responses (longitudinal bending moment and deflection at the mid-span) of the box girder and was referred to as the global IM. The global IM is rational for the flexural design of the main girders. However, for the deck slabs, the degree to which the internal forces are amplified due to the dynamic effect of moving vehicles may be different from that for the main girders. Thus, the application of the global IM to the design of bridge decks may be unreasonable and thus needs further investigations. For this reason, the local IM was proposed in this study to account for the dynamic increment of the transverse bending moment in the deck slab. The transverse strain responses of L1 to L6 were used to calculate the local IMs such that a total of six local IMs were computed for each deck slab.

In the following part of this section, the numerical analysis will be presented as follows: the typical time histories of the dynamic bridge responses will be presented and analyzed; a dynamic impact analysis will be conducted where the IMs for the two load cases are evaluated separately; a parametric study will be performed where the relationship between the IM and three important parameters is examined in details.

4.2. Dynamic responses of bridges

Figure 5 presents the response time histories of Bridge 3 under the average road surface condition. The responses were obtained under Load Case 2 in which the vehicle was set to run at 30 km/h. The time histories of the local strains at L1 and L5 are shown in Figure 5(a) and (b) while the time history of the global strain at G1 is shown in Figure 5(c). The bridge dynamic responses were obtained by using the numerical method presented before while the static responses were obtained from the simulation of a quasi-static test where the vehicle was set to travel across the bridge at a crawl speed (<1 m/s). Furthermore, also given in Figure 5 are the corresponding response histories in frequency domain. It can be seen from Figure 5(c) that, one particular mode of low frequency that corresponds to the first bending mode of the bridge, dominates the global dynamic response. However, for the local dynamic bridge responses, although notable contribution from the first bending mode of the bridge can still be identified, a significant contribution arises from the higher frequencies that correspond to the local vibrations of the deck slab. Figure 6 shows two typical modes of local vibrations. The difference in the spectral analysis indicated that the global and local bridge responses were dominated by different vibration modes.

4.3. Dynamic impact analysis

Previous studies have investigated a number of parameters that have an impact on the IM, including the road surface condition, bridge span length, dynamic characteristics of the vehicle and bridge, vehicle speed, vehicle weight, vehicle loading position, etc, (Wang and Huang, 1992; Cantieni, 1983; Green et al., 1995; Brady et al., 2006; Ashebo et al., 2007). In the present study, five bridges of different span lengths were adopted to investigate the relationship between the span length and IM; seven vehicle speeds ranging from 30 km/h to 120 km/h, with an interval of 15 km/h, were used to examine the relationship between the vehicle speed and IM; four different road surface conditions according to the ISO specification (ISO, 1995), i.e., very good, good, average and poor, were considered to study the relationship between the road surface condition and IM. The program was set to run twenty times with twenty sets of randomly generated road surface profiles under each given road surface condition and vehicle speed for each bridge. The average value of the twenty IMs was then used for the analysis. The reason for using twenty simulations is that the coefficient of variation of the impact factors obtained from twenty simulations was calculated to be less than ten percent and thus the number of twenty was considered to be sufficient.

The simulated IMs under Load Cases 1 and 2 for each bridge are plotted against the vehicle speed in Figure 7 where the IM at each speed is the average of the four road surface conditions. It can be seen from the figure that: (1) for Bridge 2, the local IMs are consistently larger than the global IMs for each vehicle speed considered; however, for other bridges, the relationship between the local and global IMs appears to be indeterminate as this relationship changes with the vehicle speed; (2) the local IMs vary between different locations on the bridge deck; nevertheless, it is interesting to see that the variation of IMs with the vehicle speed at the same cross-section follows a similar trend; (3) under Load Case 2, the IMs at symmetric locations of the deck slabs (i.e., L2 and L3, and L5 and L6) are equal to each other since the vehicle loading was applied at the central position of the deck slabs.

In addition, Figure 7 shows that the global strain based IMs are smaller than the global deflection based IMs. Similar findings were also reported by some researchers (Li et al., 2008; Huang, 2001; Szurgott et al., 2011). Nonetheless, other researchers (Fafard et al., 1998; Senthilvasan et al., 2002; Aluri et al., 2005) reported opposite findings that the IMs based on bending moment are greater than those based on deflection. From the design point of view, the IM is used to amplify internal forces and thus it seems inappropriate to adopt the IMs calculated from displacement for design.

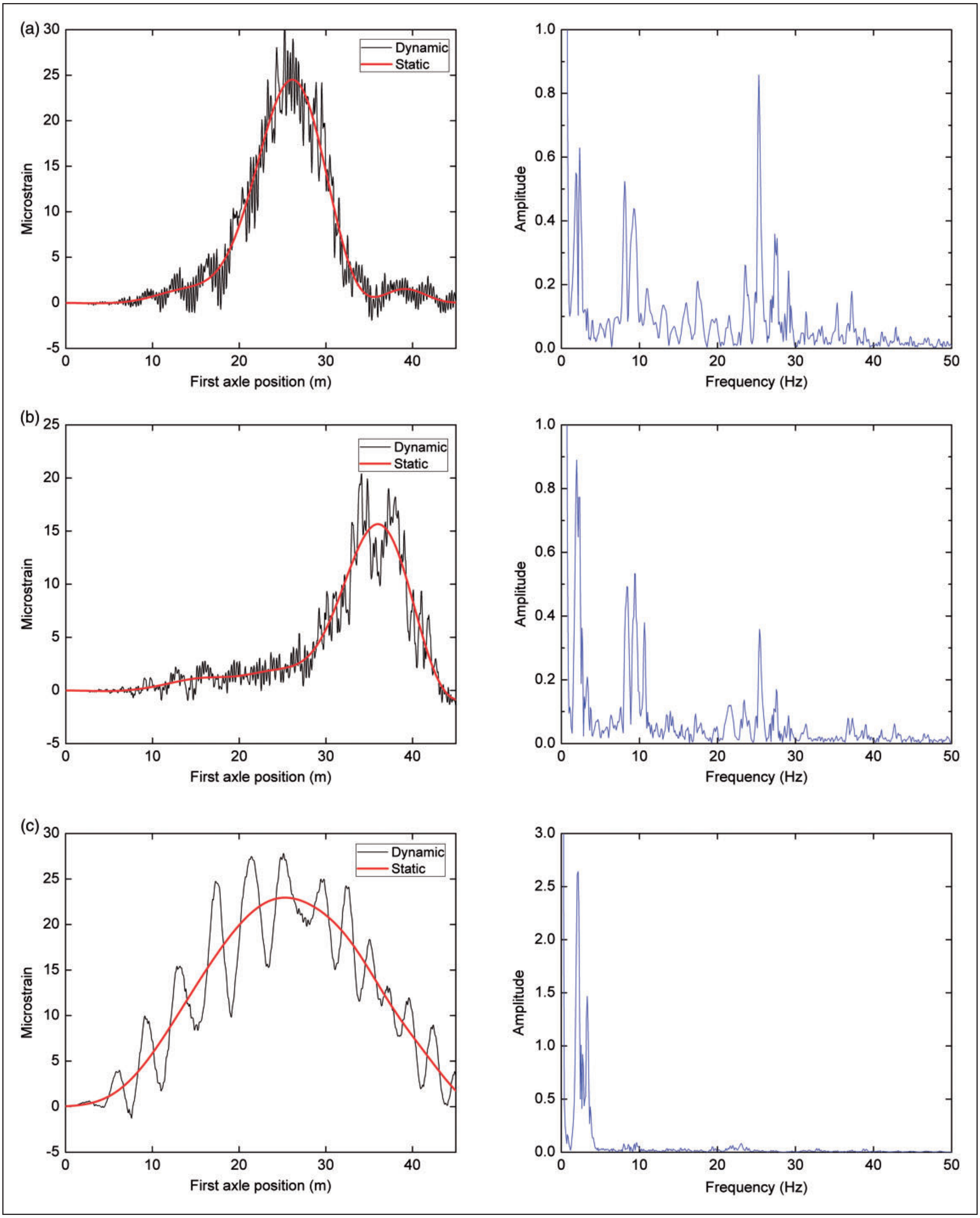

Figure 5. Typical response histories of Bridge 3 in time and frequency domain (Load Case 2): (a) transverse strain at L1, (b) transverse strain at L5 and (c) longitudinal strain at G1.

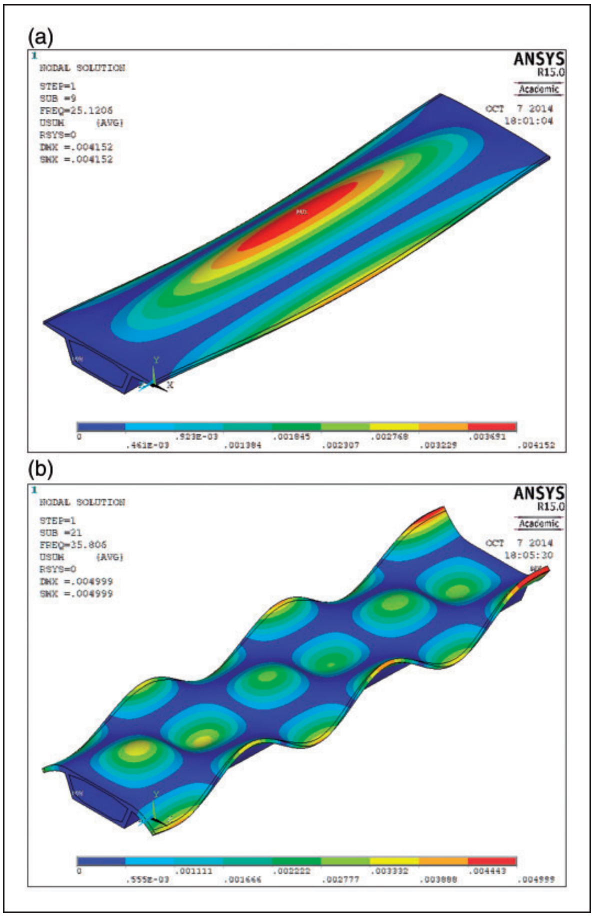

Figure 6. Typical local vibration modes of Bridge 3: (a) the 9th mode (f = 25.12 Hz) and (b) the 21th mode (f = 35.81 Hz).

4.4. Parametric study

4.4.1. Vehicle speed. Vehicle speed has been regarded as an important parameter influencing the IM. However, the relationship between the vehicle speed and IM is a complicated issue to interpret. Many researchers (Deng and Cai, 2010; Green et al., 1995; Laman et al., 1999; Azimi et al., 2011) have reported a somewhat indefinable relationship between the vehicle speed and IM.

In the present study, the variation of IMs with the vehicle speed does not follow a clear pattern, as can be seen from Figure 7. In order to gain a better understanding of the relationship between the two variables, correlation coefficients were computed for each location and the results are given in Table 3. In statistics, the correlation coefficient is a numeric measure of the linear dependence between two variables. The coefficient ranges from −1 to 1, where a coefficient of −1 or 1 indicates an absolute negative and positive correlation while a coefficient of 0 means no linear correlation. From Table 3, it can be seen that the correlation coefficients vary in an irregular manner between different locations and bridges. Nevertheless, the correlation between the vehicle speed and IM is generally weak, suggesting that the vehicle speed is not a good indicator of the IM.

4.4.2. Bridge span length. The average IMs of each road surface condition obtained from both load cases considering all vehicle speeds are plotted against the bridge span length in Figure 8 which shows the overall variation of IMs with the bridge span length. It can be seen that the local IM declines almost linearly as the span length increases. This linear relationship could have significant implication for the design of bridge deck slabs: the IM of the transverse bending moments in the deck slab may be expressed as a simple function of the bridge span length. However, the variation of the global IM with the span length seems to be significantly different: the global IM first drops radically as the span length increases from 24 m to 32 m and then increases as the span length increases from 32 m to 48 m after which it decreases again. This variation trend, to some extent, is contradictory to the traditional understanding that impact factor usually decreases with the increase of the bridge span length as specified in some bridge design codes.

Nevertheless, similar observations were also made by some researchers (Schwarz and Laman, 2001; Li, 2005; Billing, 1984). This is probably because the fundamental bending frequencies of Bridges 1 (7.92 Hz) and Bridge 4 (2.18 Hz) are close to the frequencies corresponding to the hopping motion of the vehicle's first axle and the bouncing of the vehicle body, respectively. In such a case, the resonance of the vehicle-bridge system occurs and the global IM can be significant. In addition, it is noted that the fundamental frequencies of Bridges 3 and 5 (3.09 Hz and 1.61 Hz) are also close to the third and first frequencies of the vehicle (2.69 Hz and 1.52 Hz); however, resonance did not occur for these two bridges. This is because the first and third frequencies of the vehicle correspond to the vibration modes of trailer rolling and tractor pitching, respectively. Therefore, while the first frequency of the vehicle is close to the fundamental bending frequency of Bridge 5, this frequency does not correspond to a vertical mode, suggesting that it will not excite the vertical vibration of the bridge and thus no resonance occurred. For Bridge 3, while the pitching mode exerts some level of vertical excitation, it is not as noticeable as the bouncing and hopping modes. Also, the frequency of 2.69 Hz is not as close to 3.09 Hz as 2.14 Hz to 2.18 Hz and 7.74 Hz to 7.92 Hz. Thus, the resonance did not occur at Bridge 3 either.

To better examine the variation trend of IMs with the bridge span length, the variation of the maximum responses and corresponding IMs with span length is

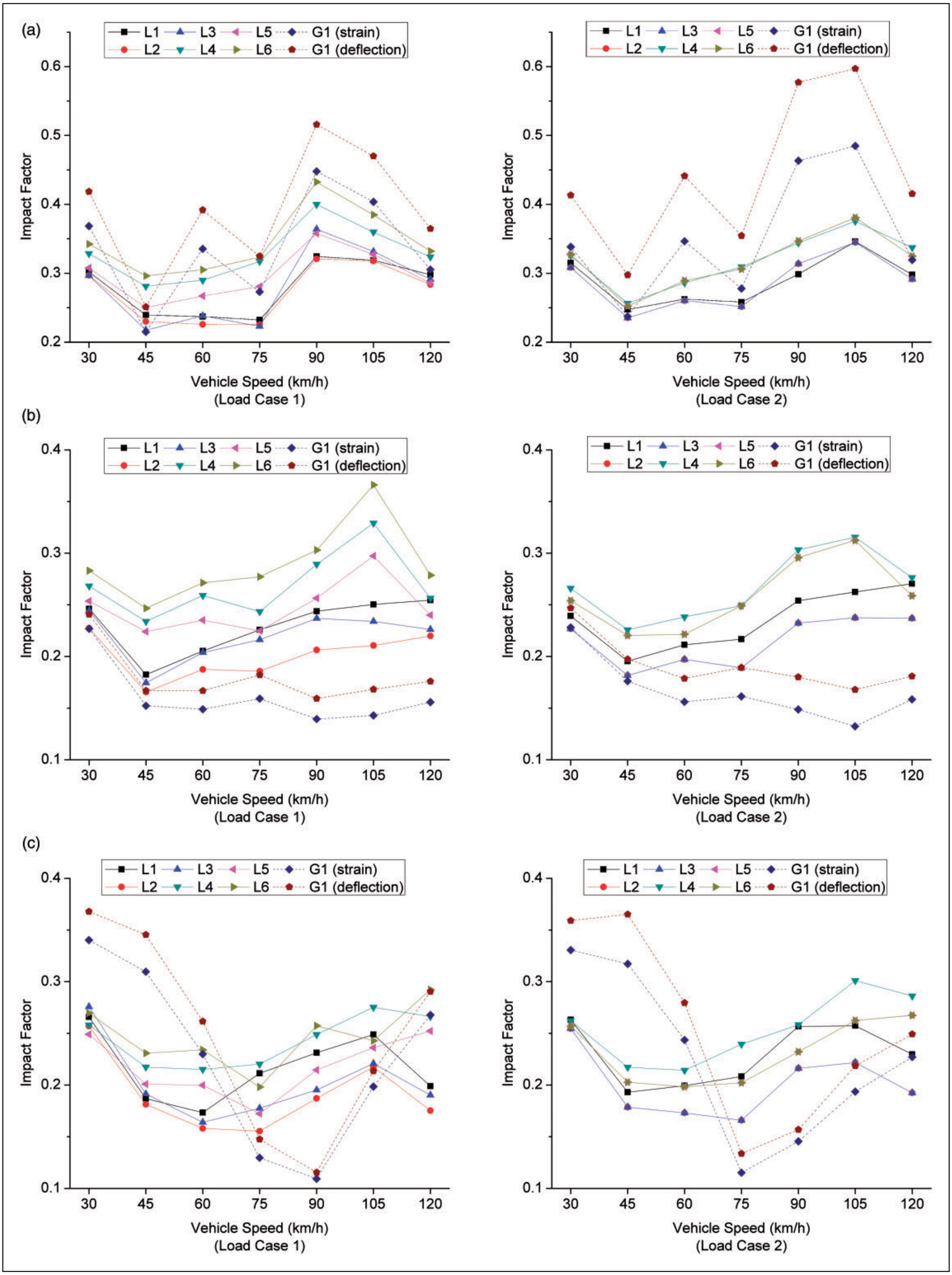

Figure 7. Variation of IM with vehicle speed for each bridge: (a) Bridge 1, (b) Bridge 2, (c) Bridge 3, (d) Bridge 4 and (e) Bridge 5.

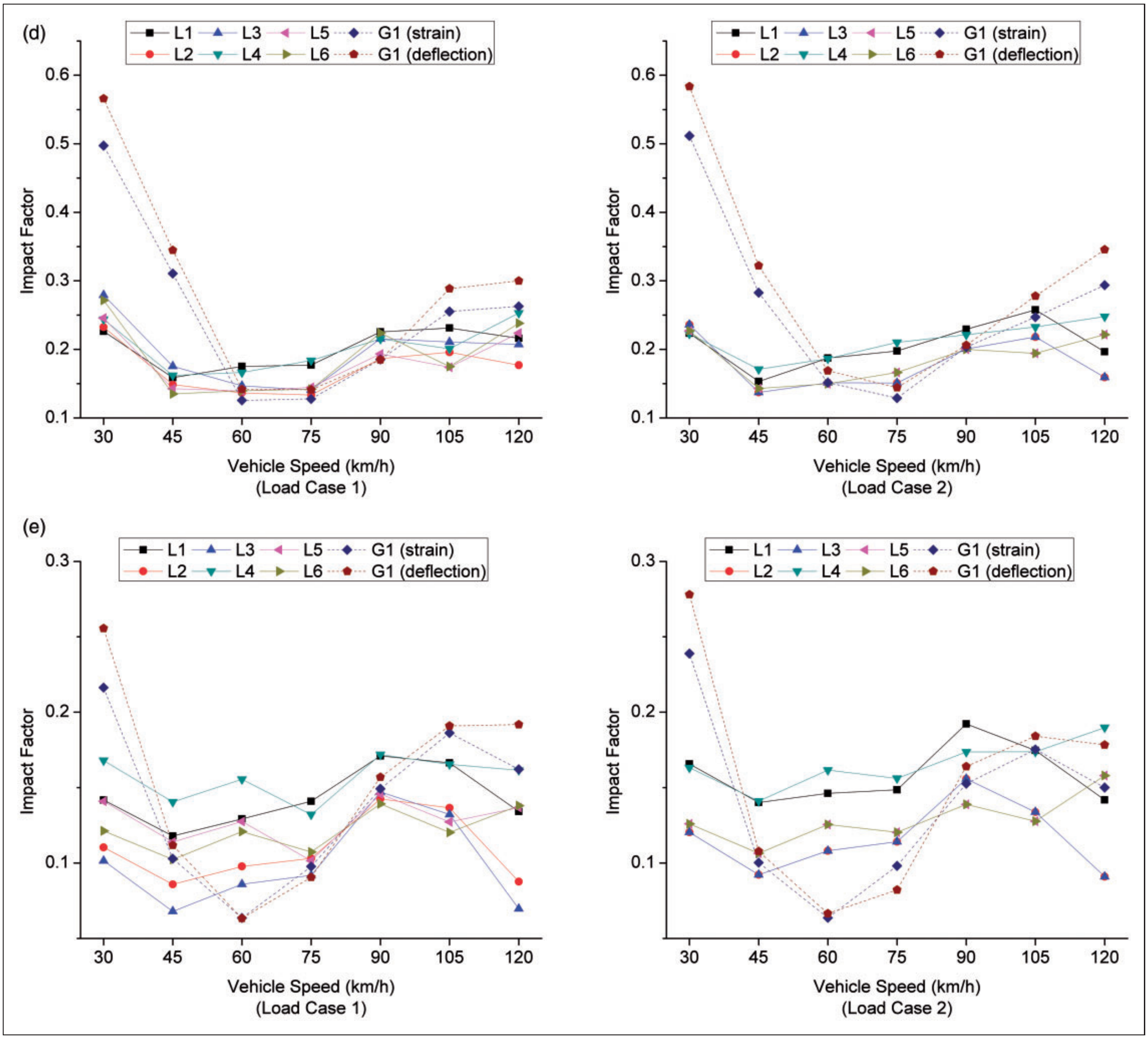

Figure 7. Continued.

Table 3. Correlation coefficients between vehicle speed and IM.

	L1	L2	L3	L4	L5	L6	G1(strain)	G1(deflection)
Bridge 1	0.4342	0.4303	0.4629	0.5910	0.4993	0.5289	0.3935	0.4501
Bridge 2	0.6651	0.4541	0.4570	0.5596	0.5311	0.5786	−0.7064	−0.6653
Bridge 3	0.0830	−0.2314	−0.2557	0.6134	0.3643	0.4006	−0.5638	−0.5815
Bridge 4	0.4185	−0.0433	−0.0889	0.4954	0.1925	0.1762	−0.4314	−0.4233
Bridge 5	0.3214	0.2059	0.1989	0.5680	0.4985	0.6765	0.0429	0.0064

shown in Figure 9. These maximum responses and IMs are the average values obtained from the simulations where the vehicle travels at 30 km/h under the average road surface condition. Despite the difference in the value of IMs, the variation trend of IM with span length in Figure 9 is consistent with that in Figure 8. For the local response, it can be seen from Figure 9(a) that while the static strain response does not change significantly with the bridge span length as expected, the dynamic strain response appears to decrease with the increase of the bridge span length, causing the decrease of the local IM. As for the global responses

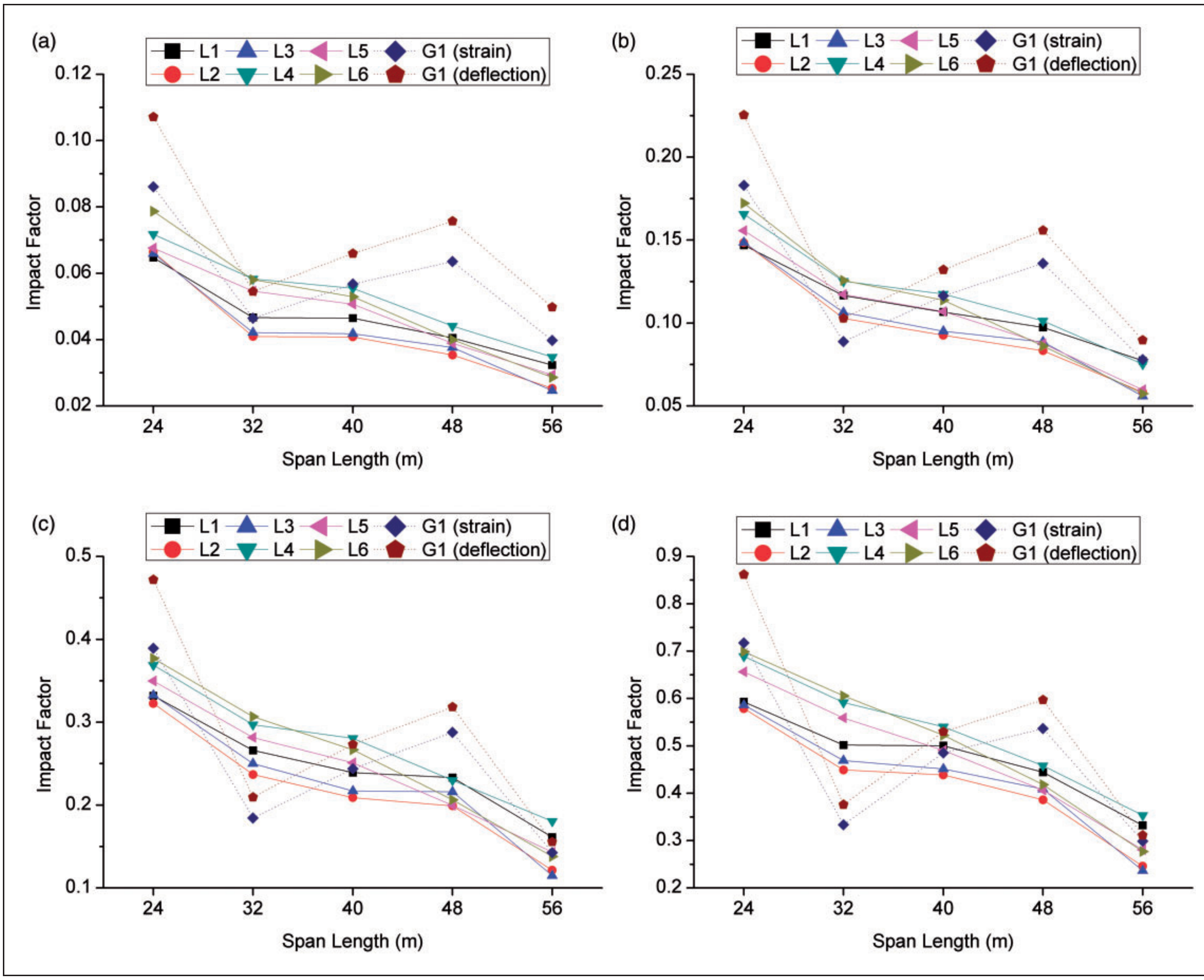

Figure 8. Variation of average IMs with the bridge span length: (a) very good surface condition, (b) good surface condition, (c) average surface condition and (d) poor surface condition.

shown in Figure 9(b), it can be seen that both the static and dynamic deflections at the bridge mid-span increase with the span length but with different magnitudes, resulting in the particular variation trend of the global IM with the span length. The different variation trends of the local and global IMs with the span length can be explained as follows: the main cause of the variation of the global IM with the span length is the resonance of the vehicle-bridge system which mainly affects the global vibration of the bridge; however, as discussed before, the major contribution to the local dynamic responses of the deck slab arises from the local vibration modes of the deck slab rather than the global vibration of the bridge. Thus, the variation of the local and global IMs with the bridge span length is different.

4.4.3. Road surface condition. Road surface roughness has been identified as a major source of excitations in the vehicle-induced bridge vibrations. Many previous studies have indicated that the IM increases as the road surface condition worsens, and the present study is no exception. Figure 10 shows the variation of the IMs with the road surface condition. It can be seen that the IMs increase almost linearly with the increase of road roughness.

In addition, the statistical parameters of the IM for different road surface conditions were calculated for each location considering all span lengths and vehicle speeds and the results are tabulated in Table 4. It can be seen that: (1) although the mean local IMs vary between different locations on the bridge deck, the variation of IMs with different locations is generally insignificant. This is consistent with the finding by Broquet et al. (2004); (2) for each road surface condition, the difference between the mean values of the local and global IMs is basically small. Furthermore, it can be seen from Table 4 that the global IMs generally have higher standard deviations than the local IMs,

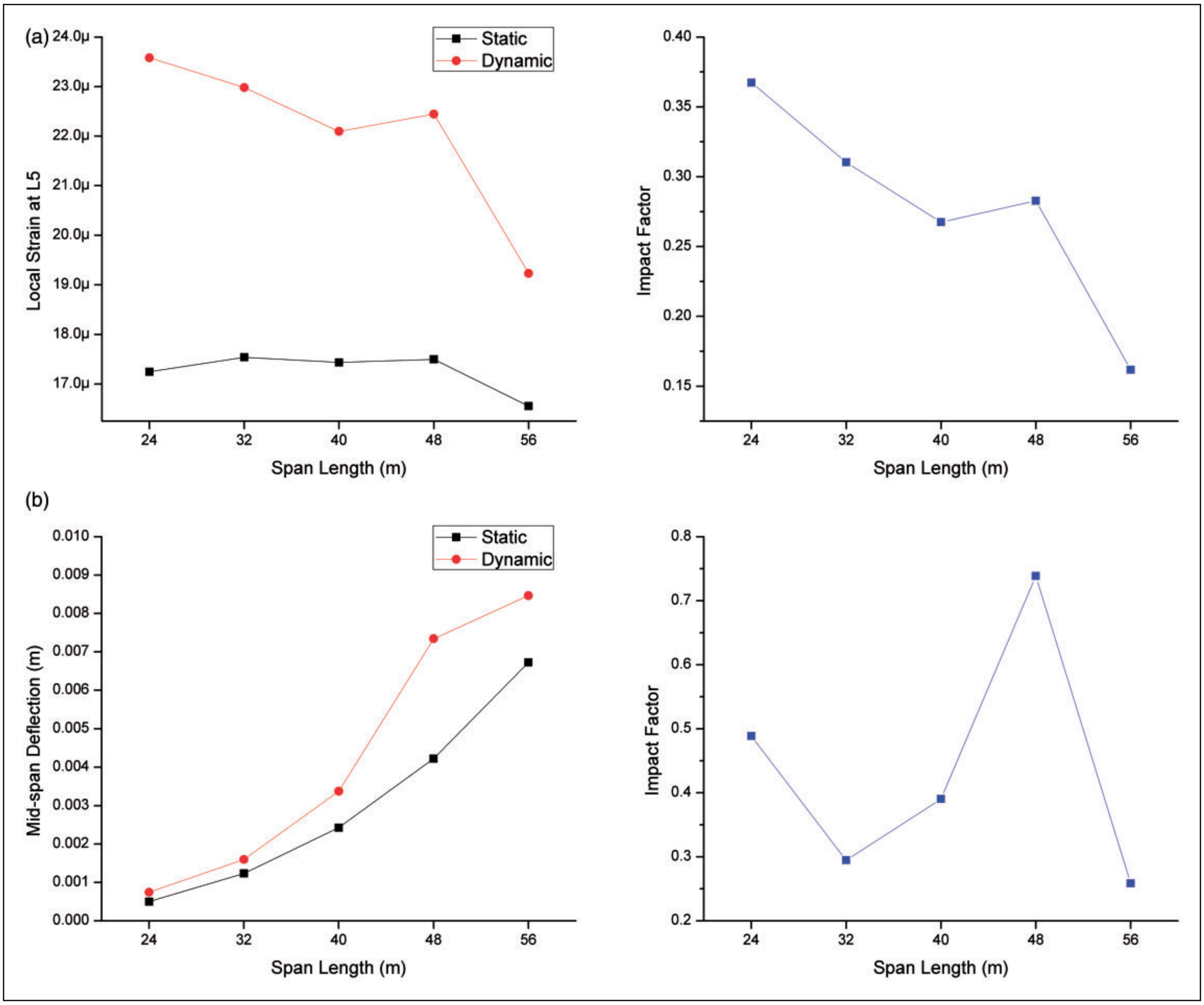

Figure 9. Variation of maximum responses and corresponding IMs with span length: (a) transverse strain and local IM at L5 and (b) deflection and global IM at G1.

suggesting the distribution of the global IM is more dispersed than that of the local IM. Moreover, the coefficients of variation (COV) for the local IMs range from 40% to 72% and the COVs for the global IMs range from 64% to 76%. The calculated COV range in this study is similar to those reported in other studies (Hwang and Nowak, 1991; Schwarz and Laman, 2001; Billing, 1984). This suggests that the IM is a nondeterministic quantity and should be determined based on statistical and probabilistic approaches.

5. Discussion on code provisions

Many bridge design codes do not differentiate the IMs for the local deck design and global bridge design. For example, the AASHTO LRFD code (AASHTO, 2012) specifies a uniform value of 0.33 for the impact of all components except for the deck joints. Similar provisions can also be found in the Canadian Highway Bridges Design Code (CSA, 2006), AS 5100-2 (Austroads, 2004), etc. Nonetheless, there are a few design codes that specify different IMs for the design of deck slabs and main girders. For example, in the previous AASHTO Standard Specification (AASHTO, 2002), the IM is specified as

$$IM = \frac{15.24}{L + 38.10} \tag{10}$$

where L is the loaded length in meters and the IM is not to exceed 0.3. For the global design of bridges, e.g., the main girders, the loaded length refers to the design span length of the bridge, while the loaded length refers to the girder spacing for the design of bridge decks. Since the girder spacing is usually much smaller than the bridge span length, the local IM will be higher than the global

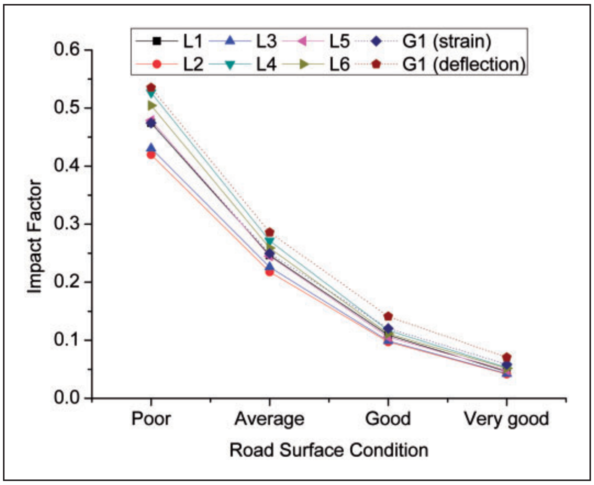

Figure 10. Variation of average IMs with road surface condition.

Table 4. Statistical parameters of IM for different road surface conditions.

Roughness	Location	Mean	Std. dev.	COV
Poor	L1	0.4743	0.1897	40.00%
	L2	0.4197	0.1934	46.08%
	L3	0.4304	0.2068	48.05%
	L4	0.5266	0.2224	42.23%
	L5	0.4788	0.2250	46.99%
	L6	0.5044	0.2464	48.85%
	G1 (strain)	0.4743	0.3073	64.79%
	G1 (deflection)	0.5352	0.3603	67.32%
Average	L1	0.2463	0.1117	45.35%
	L2	0.2178	0.1145	52.57%
	L3	0.2261	0.1229	54.36%
	L4	0.2714	0.1266	46.65%
	L5	0.2450	0.1249	50.98%
	L6	0.2590	0.1393	53.78%
	G1 (strain)	0.2496	0.1715	68.71%
	G1 (deflection)	0.2858	0.1984	69.42%
Good	L1	0.1089	0.0545	50.05%
	L2	0.0971	0.0568	58.50%
	L3	0.0989	0.0603	60.97%
	L4	0.1170	0.0612	52.31%
	L5	0.1054	0.0620	58.82%
	L6	0.1111	0.0684	61.57%
	G1 (strain)	0.1204	0.0875	72.67%
	G1 (deflection)	0.1411	0.1002	71.01%
Very good	L1	0.0461	0.0283	61.39%
	L2	0.0418	0.0296	70.81%
	L3	0.0424	0.0308	72.64%
	L4	0.0529	0.0316	59.74%
	L5	0.0482	0.0324	67.22%
	L6	0.0517	0.0357	69.05%
	G1 (strain)	0.0585	0.0445	76.07%
	G1 (deflection)	0.0706	0.0497	70.40%

IM. In fact, the girder spacing is generally small enough to result in the maximum IM of 0.3. Coincidentally, the Bridge Manual (NZTA, 2013) by the New Zealand Transport Agency also specifies an IM of 0.3 for calculating the design moments in deck slabs.

From Table 4, it can be seen that when the road surface condition is better than "poor", both the local and global IMs are well below the value of 0.33, implying that the impact provision in the AASHTO LRFD code (AASHTO, 2012) can be safely applied to the strength design of deck slabs of concrete box-girder bridges. However, this implication does not mean that the local IM and global IM can be treated as the same since they are different in certain ways as discussed earlier.

It is stated in the commentary of the AASHTO LRFR code (AASHTO, 2003) that 0.33 is a conservative value to account for certain distressed approach and deck conditions. However, it can be seen that under the poor road surface condition, the mean values of both the local and global IMs are around 0.5 which exceeds the specified value of 0.33 by the AASHTO LRFD code (AASHTO, 2012). This is understandable since the bridge design cannot be based on the poor surface condition as it will be too conservative. However, this phenomenon should still be noted in the performance evaluation of old bridges with distressed surface conditions. In light of this, the regular maintenance of the roadway is a very cost-effective approach to reduce the dynamic impact effect of moving vehicles in bridge management.

6. Conclusions

The main purpose of this study was to assess the local dynamic impact factor of bridge deck slabs. For this purpose, a dynamic impact analysis was carried out on a series of prestressed concrete box-girder bridges under the HS20 truck loading by using a fully computerized bridge-vehicle coupled model. The local IMs and global IMs were defined at different locations based on different responses. The relationship between the IM and three important parameters including the road surface condition, bridge span length, and vehicle speed was examined. The comparison between the global and local IMs was also made. Based on the results obtained from the numerical analysis, the following conclusions can be drawn:

1. The global and local dynamic responses are dominated by different vibration modes. The global

dynamic bridge response is dominated by one particular mode, i.e., the first vertical bending mode of the bridge. However, the local dynamic responses of the bridge deck are controlled by the local vibration modes of the bridge deck.
2. The relationship between the vehicle speed and IM seems to be irregular as the increase of velocity does not guarantee either an increase or decrease of the IM. A correlation analysis shows that the vehicle speed is not a good indicator of the IM.
3. The local IMs decrease almost linearly with the increase of the span length due to the decrease of the local dynamic vibrations. However, no such tendency exists between the global IMs and span length due to the resonance of the vehicle-bridge system.
4. Both the local and global IMs increase significantly as the road surface condition deteriorates and there exists a linear correlation between the road surface condition and IM.
5. The variation of the local IMs with different locations within the same cross section of the bridge deck is insignificant and the distribution of the global IM is more dispersed than the local IM. The large value of COV also suggests that the IM is not a deterministic quantity.
6. The impact provision in the AASHTO LRFD code can be safely applied to the strength design of concrete deck slabs of box-girder bridges, but is not conservative for the evaluation of existing bridges with poor deck surfaces. Nevertheless, the applicability of this provision to the deck slabs of other types of bridges still requires further research.

Conflict of interest

The authors report no conflict of interest.

Funding

The authors gratefully acknowledge the financial support provided by the National Natural Science Foundation of China (grant numbers 51208189 and 51478176) and Excellent Youth Foundation of Hunan Scientific Committee (grant number 14JJ1014).

References

Aluri S, Jinka C and GangaRao H (2005) Dynamic response of three fiber reinforced polymer composite bridges. *Journal of Bridge Engineering* 10: 722–730.

American Association of State Highway and Transportation Officials (AASHTO) (1994) *LRFD bridge design specifications*. Washington DC, USA.

American Association of State Highway and Transportation Officials-Precast/Prestressed Concrete Institute-American Segmental Bridge Institute (AASHTO–PCI–ASBI) (1997) *Segmental box girder standards*. Washington DC, USA.

American Association of State Highway and Transportation Officials (AASHTO) (2002) *Standard specifications for highway bridges*. Washington DC, USA.

American Association of State Highway and Transportation Officials (AASHTO) (2003) *Guide manual for condition evaluation and load and resistance factor rating (LRFR) of highway bridges*. Washington DC, USA.

American Association of State Highway and Transportation Officials (AASHTO) (2012) *LRFD bridge design specifications*. Washington DC, USA.

Ashebo DB, Chan THT and Yu L (2007) Evaluation of dynamic loads on a skew box girder continuous bridge Part II: Parametric study and dynamic load factor. *Engineering Structures* 29: 1064–1073.

Austroads (2004) *AS 5100: Bridge design standard Part 2: Design load*. Sydney, Australia.

Azimi H, Galal K and Pekau OA (2011) A modified numerical VBI element for vehicles with constant velocity including road irregularities. *Engineering Structures* 33: 2212–2220.

Billing JR (1984) Dynamic loading and testing of bridges in Ontario. *Canadian Journal of Civil Engineering* 11: 833–843.

Brady S, O'Brien E and Žnidarič A (2006) Effect of vehicle velocity on the dynamic amplification of a vehicle crossing a simply supported bridge. *Journal of Bridge Engineering* 11: 241–249.

Broquet C, Bailey S, Fafard M and Brühwiler E (2004) Dynamic behavior of deck slabs of concrete road bridges. *Journal of Bridge Engineering* 9: 137–146.

Canadian Standards Association (CSA) (2006) *Canadian highway bridge design code*. Ontario, Canada.

Cantieni R (1983) Dynamic load tests on highway bridges in Switzerland–60 years of experience of EMPA. *EMPA Report No. 211*. Swiss Federal Laboratories for Materials Testing and Research. Dübendorf, Switzerland.

Deng L and Cai CS (2010) Development of dynamic impact factor for performance evaluation of existing multi–girder concrete bridges. *Engineering Structures* 32: 21–31.

Fafard M, Laflamme M, Savard M and Bennur M (1998) Dynamic analysis of existing continuous bridge. *Journal of Bridge Engineering* 3: 28–37.

Green M, Cebon D and Cole D (1995) Effects of vehicle suspension design on dynamics of highway bridges. *Journal of Structural Engineering* 121: 272–282.

Huang D, Wang T and Shahawy M (1993) Impact studies of multigirder concrete bridges. *Journal of Structural Engineering* 119: 2387–2402.

Huang D, Wang T and Shahawy M (1995) Vibration of thin–walled box–girder bridges excited by vehicles. *Journal of Structural Engineering* 121: 1330–1337.

Huang D (2001) Dynamic analysis of steel curved box girder bridges. *Journal of Bridge Engineering* 6: 506–513.

Hwang E and Nowak A (1991) Simulation of dynamic load for bridges. *Journal of Structural Engineering* 117: 1413–1434.

International Organization for Standardization (ISO) (1995) *Mechanical vibration-road surface profiles–reporting of measured data*. ISO 8608: 1995(E), Geneva: ISO.

Laman J, Pechar J and Boothby T (1999) Dynamic load allowance for through-truss bridges. *Journal of Bridge Engineering* 4: 231–241.

Li H (2005) *Dynamic response of highway bridges subjected to heavy vehicles*. PhD Dissertation. Tallahassee, FL: Florida State University.

Li H, Wekezer J and Kwasniewski L (2008) Dynamic response of a highway bridge subjected to moving vehicles. *Journal of Bridge Engineering* 13: 439–448.

New Zealand Transport Agency (NZTA) (2013) *Bridge manual*. Wellington, New Zealand.

Schwarz M and Laman J (2001) Response of prestressed concrete I-girder bridges to live load. *Journal of Bridge Engineering* 6: 1–8.

Senthilvasan J, Thambiratnam DP and Brameld GH (2002) Dynamic response of a curved bridge under moving truck load. *Engineering Structures* 24: 1283–1293.

Szurgott P, Wekezer J, Kwasniewski L, Siervogel J and Ansley M (2011) Experimental assessment of dynamic responses induced in concrete bridges by permit vehicles. *Journal of Bridge Engineering* 16: 108–116.

Wang T, Huang D and Shahawy M (1996) Dynamic behavior of continuous and cantilever thin-walled box girder bridges. *Journal of Bridge Engineering* 1: 67–75.

Wang T and Liu C (2000) Influence of heavy trucks on highway bridges. *Rep. No. FL/DOT/RMC/ 6672–379*. Tallahassee, FL: Florida Department of Transportation.

Wang T and Huang D (1992) Cable-stayed bridge vibration due to road surface roughness. *Journal of Structural Engineering* 118: 1354–1374.